NIH Public Access
Author Manuscript
Oral Surg Oral Med Oral Pathol Oral Radiol. Author manuscript; available in PMC 2014 February 01.

Published in final edited form as:
Oral Surg Oral Med Oral Pathol Oral Radiol. 2013 February ; 115(2): 201–211. doi:10.1016/j.oooo.2012.09.008.

Onset of mandible and tibia osteoradionecrosis – a comparative pilot study in the rat

Monika Damek-Poprawa, PhD[1], **Stefan Both, PhD**[2], **Alexander C. Wright, PhD**[3], **Amit Maity, MD,PhD**[4], and **Sunday O. Akintoye, BDS,DDS,MS**[5,*]

[1]Department of Microbiology, School of Dental Medicine, University of Pennsylvania, Philadelphia, PA 19104, USA

[2]Division of Medical Physics, Department of Radiation Oncology, School of Medicine, University of Pennsylvania, Philadelphia PA 19104, USA

[3]Department of Radiology, School of Medicine, University of Pennsylvania, Philadelphia, PA 19104

[4]Division of Radiation Biology, Department of Radiation Oncology, School of Medicine, University of Pennsylvania, Philadelphia PA 19104, USA

[5]Department of Oral Medicine, School of Dental Medicine, University of Pennsylvania, Philadelphia, PA 19104, USA

Abstract

Objectives—Osteoradionecrosis (ORN) is common in the jaws following radiotherapy. We hypothesized that mandible is more susceptible to ORN than tibia based on site-disparity in hypoxic-hypocellular-hypovascular tissue breakdown.

Study Design—Twelve rats received 50 Gy irradiation to mandible or tibia; 4 of 12 rats further received minor surgical trauma to the irradiated sites. Structural and cellular skeletal changes were assessed with computer tomography, histology and immunostaining.

Results—Mandible developed ORN with 70% mean bone loss 10 weeks post-irradiation ($p < 0.05$) while tibia was structurally and radiological intact for 20 weeks post-irradiation. Hypocellularity, hypoxia and oxidative stress were higher in irradiated mandible ($p < 0.001$) than tibia ($p < 0.01$) but vascular damage was similar at both skeletal sites. Combined effects of radiation and minor trauma promoted mandibular alveolar bone loss and tibial fracture

Conclusion—ORN has a more rapid onset in mandible relative to tibia in the rat

Keywords

Osteoradionecrosis; Hypovascular; Hypocellular; Radiotherapy; Oxidative stress; Animal model

*Corresponding Author: Sunday O. Akintoye BDS, DDS, MS, University of Pennsylvania School of Dental Medicine, Department of Oral Medicine, Robert Schattner Room 211, 240 S. 40th Street, Philadelphia PA 19104, Office: 215-898-9932: Fax: 215-573-7835. akintoye@dental.upenn.edu.

DISCLOSURES
The authors declare that they have no conflict of interest.

INTRODUCTION

Ionizing radiation is commonly used to treat head and neck cancers; however, osteoradionecrosis (ORN) is a major complication. Incidence of ORN can be as high as 10% or higher depending on dose of radiation and comorbid factors [1–3]. ORN is characterized by tissue dehiscence, chronic bone devitalization, hypocellularity and osteolysis. Histological changes in irradiated bone include decreased osteocyte count, empty osteocyte lacunae as well as increased osteoclast number and activity [1, 4]

While ORN is a common complication of cancer radiotherapy in the head and neck, post-irradiation skeletal fractures and delayed healing are more common in axial and appendicular bones. The events associated with this clinical disparity have not been directly assessed in a small animal model [5]. Additionally, clinical reports suggest that radiation-induced bone damage progresses much more rapidly to necrosis in orofacial bones, but site-specific radiation-induced cellular and structural changes that potentially promote jaw susceptibility to radiation damage are yet to be fully elucidated [5–7]. Currently ORN is associated with radiation-induced 'hypoxic-hypocellular-hypovascular' tissue followed by tissue breakdown and chronic non-healing wound in which metabolic and structural precursor demands exceed supply [8]. This hypothesis has also not been conclusively clarified.

Bone marrow stromal cells (BMSCs) supply progenitor cells vital for bone healing, but skeletal site disparity in radio-responsiveness of BMSCs suggest that oral and long bones may be differentially susceptible to ORN [9]. Developing a small animal model to study skeletal site-specific pathophysiological mechanisms of ORN is often hindered by technical difficulties associated with targeting radiation to specific sites in the jaw of small animals. This is because external beam radiation of rodent jaws is often complicated by collateral damage to other craniofacial structures and animals do not survive long enough for long-term follow-up [10]. When radiation is delivered via a catheter attached to a remote afterloader microSelectron high dose rate (HDR) machine, it is possible to irradiate defined skeletal sites in small animals with minimal collateral damage to adjacent structures. Since orofacial and long bones have different embryological origins and BMSCs that reside in them are skeletal site specific in terms of their responsiveness to irradiation [9], we used a rat ORN model to test the hypothesis that mandible (oral bone) is more susceptible to ORN than tibia (appendicular bone).

MATERIALS AND METHODS

Animal irradiation and surgical procedures

Localized high dose rate (HDR) radiation was delivered by brachytherapy to female NIH-RNU 6 week-old rats [(n = 8), Charles Rivers Laboratories (Wilmington, MA, USA)] under anesthesia induced with ketamine (37 mg/kg body weight) and medetomidine (0.5 mg/kg body weight). Animal protocol was approved by University of Pennsylvania Animal Care and Use Committee. Due to previous reports of specie and skeletal site differences at low radiation doses, [9, 11, 12] we chose NIH-RNU rats so that graft therapy for ORN will be feasible in follow-up studies; we also performed pre-study survival dose response with 30 – 60 Gy (data not shown) to ensure that animals will survive, and spontaneous ORN will develop[10, 13]. Hence, 50 Gy, a clinically relevant dose, was delivered to either right body of the mandible or right proximal tibia through a 150 mm long by 2 mm close-tipped lumen catheter (5F, Nucleotron BV, Veenendaal, The Netherlands) positioned cutaneously. The catheter was attached to a remote afterloader microSelectron HDR machine having a 10Ci Ir192 source (Nucleotron BV, Veenendaal, The Netherlands). Pretreatment planning involved preliminary *in vivo* microscopic computed tomography (micro-CT) to calculate

dosimetry and depth of radiation penetration (Figs. 1A – D) using computer assisted standard dose-calculation planning system (PLATO-Brachytherapy Version 14.2.6 Nucleotron BV, Veenendaal, The Netherlands). Each animal's non-irradiated left mandible or left tibia served as respective control sites. Post irradiation, anesthesia was reversed with atipamezole (1 mg/kg body weight). Animals were maintained on liquid diet (PMI® micro stabilized rodent liquid diet Cat # LD101, TestDiet, Richmond IN) and evaluated twice weekly for signs of post-radiation complications; these included swelling, redness, moist desquamation and ulceration. When animals showed any sign of distress, a staff veterinarian gave analgesic medication. Four of the 12 animals were further challenged with minor surgical trauma to the irradiated sites 8 weeks post-irradiation as follows (Fig. 1E): Under anesthesia as above, a tungsten carbide dental bur (#556) attached to a portable dental handpiece unit was used to create 0.1 mm diameter cortical hole in the right mandibular buccal plate adjacent to the first molar (n=2) or in the proximal lateral cortical plate of the right tibia (n=2). The animals were monitored twice weekly for post-irradiation complications.

In vivo microscopic computed tomography (micro-CT)

Longitudinal skeletal changes were monitored with *in vivo* micro-CT at 4-week intervals for 20 weeks (Fig. 1E). Animals were anesthetized as described above for micro-CT scanning using MicroCAT II (ImTek Inc. Knoxville TN) and the following parameters: 80 kVp, 500 μA, 375 ms exposure and 360 projections. Gantry was a clear plastic supplied by manufacturer and images were reconstructed with manufacturer-supplied software (MicroCAT: Image Reconstruction, Visualization, & Analysis) using Feldkamp algorithm with a Shepp-Logan Filter [14]. Voxel size was 103 μm × 103 μm × 103 μm cubic voxels. Radiation damage based on relative voxel intensity of complimentary anatomic regions of interest (ROI) in irradiated versus non-irradiated mandibles were assessed with AMIDE (A Medical Image Data Examiner, version 0.8.19) [15]. Similarly, bone loss based on percentage of regional bone volume relative to total volume was also assessed in complimentary ROI in irradiated versus non-irradiated sites [16].

Ex vivo high-resolution micro-CT of skeletal samples

After rats were euthanized with carbon dioxide asphyxiation, the mandible and tibia of each animal were carefully dissected free of soft tissues, fixed with 4 % paraformaldehyde (PFA) in PBS (pH 7.4). Samples were immersed in water in a plastic sample tube for *ex vivo* micro-CT scanning using an eXplore Locus SP specimen scanner (GE Healthcare, Waukesha, WI, USA): 80 kVp, 80 μA, 250-μm Al filter, 760 views, 0.5° steps, 1.7 sec exposure, 2 × 2 detector bin mode, 4 frame averages, and 2 hour scan time. Raw data were reconstructed at 16 μm or 29.5 μm isotropic resolution via a modified Feldkamp algorithm [14]. Reconstructed images were viewed with OsiriX software (www.osirix-viewer.com), which allowed multi-planar reformatting at arbitrary oblique slices, maximum intensity projection and volume rendering. For volume rendering, a bone/muscle color palette was chosen together with a logarithmic inverse opacity function to enhance subtle intensity differences in soft tissue, enamel, dentin and bone.

Histology and immunostaining

After high resolution micro-CT, the PFA-fixed skeletal parts were decalcified with 10 % EDTA in PBS (pH 8.0), embedded in paraffin and 5 μm tissue sections were stained with hematoxylin/eosin (H&E) for histological evaluation. To determine severity of osteonecrosis, we quantified dead osteocytes in histological sections based on number of empty lacunae (without stained nucleus) per unit area and evaluated adipocyte density using ImageJ version 1.45b (National Institutes of Health, Bethesda MD) as previously described [17, 18]. Furthermore, tissue sections were deparaffinized and immunostained with

the following primary antibodies: rabbit polyclonal anti-human vascular endothelial factor (VEGF, 1:1000 dilution, catalogue # PC315, EMD4Biosciences, Gibbstown, NJ), anti-human fibroblast growth factor-basic (bFGF, 1:100 dilution, catalogue # PC16, EMD4Biosciences, Gibbstown, NJ), anti-human malondialdehyde (MDA, 1:5000 dilution, catalogue # ab6463, Abcam, Cambridge MA), and mouse monoclonal anti-human hypoxia inducible factor 1α (HIF1α, 1:1000 dilution, catalogue # ab463, Abcam, Cambridge, MA). Immunoreactivity of primary antibodies was visualized with DakoCytomation EnVision+ DualLinksystem-HRP (DAB+) kit (catalogue # K4065, Dako, North America, Carpinteria, CA) following manufacturer's recommendations. Negative controls omitted primary antibodies substituted with non-immune serum for rabbit antibodies and IgG isotype control for monoclonal antibody. Quantitative angiographic assessment of immunostained blood vessels was performed with ImageJ version 1.45b (National Institutes of Health, Bethesda MD).

Statistical analysis

Data variables from irradiated and non-irradiated sites were expressed as mean ± standard deviation. Results were analyzed and compared by two-way analysis of variance (ANOVA) followed by post hoc comparisons with Holm–Sidak test using SigmaStat 3.1 statistical package (Systat Software, Inc., Chicago, IL). Statistical significance was set at $p < 0.05$.

RESULTS

Twelve animals were involved in this pilot study of which n = 4 (33.3%) were further challenged with minor surgical trauma. The HDR afterloader delivered a dose of 50 Gy that penetrated the full diameter of mandible and tibia (Figs. 1A – D); it also confined radiation-induced erythema and dermatitis to the irradiated sites without extensive collateral damage to other structures (Figs. 2A and B). In the right mandible, erythema became associated with edema and pronounced unilateral swelling around the irradiated region (Figs. 2C and D). Soft tissue ulceration and osteonecrosis with bone sequestrum developed in the mandible within 10 weeks post-irradiation (Figs. 2E and F). Rats irradiated in the mandible also displayed slower and variable increase in body weight (Fig. 2G) and were therefore euthanized at 10 weeks. Rats irradiated in the tibia did not display clinical signs of osteonecrosis or distress, so they were followed up for 20 weeks post-irradiation.

In vivo micro-CT revealed a necrotic region characteristic of ORN in right mandible including opacification of pulp chambers of right lower incisor (Figs. 3A and B), but no distinct radiological features of ORN were present in the tibia up to 20 weeks before euthanasia (Fig. 3C). Quantitative analysis of radiologically observable bone in irradiated mandible indicated up to 70% reduction in bone tissue compared with non-irradiated control side ($p < 0.05$, Figs.3D and E). Three-dimensional volume rendering of micro-CT images demonstrated advanced lingual, periodontal, trabecular and cortical bone loss associated with pulp chamber opacification of incisor and molar teeth in the irradiated region (Figs. 3F, G, H and I). There was a mean difference of 50% alveolar bone loss on the lingual ($p < 0.001$) and buccal ($p< 0.01$) surfaces of the first molar in irradiated versus non-irradiated mandible. Irradiation also caused ankylosis of right incisor with consequent delayed eruption (Fig. 3J) that apparently impacted feeding and erratic weight gain (Fig. 2G). Histological features of ORN in mandible included necrotic acellular bone with loss of osteocytes, formation of sequestrum, ruptured vasculature with extravasated erythrocytes and eosinophilic amorphous ground substance infiltrated by basophilic cells (Figs. 4A – 4E). Irradiated right mandibular incisor became sclerotic with warped dentin and loss of pulpal tissues consistent with pulp necrosis (Fig. 4C). Histology of irradiated tibia showed distorted growth plate architecture, trabecular micro-fractures and altered marrow elements consisting of marked adipogenesis, reduced hematopoietic and stromal cells, coalesced adipocytes and

fatty infiltration of inter-trabecular marrow spaces (Figs. 4F – 4J). Both irradiated mandible ($p < 0.001$) and tibia ($p < 0.01$) ORN displayed empty osteocyte lacunae characteristic of dead osteocytes (Fig. 4K) but there was a discordant effect on adipocytic differentiation. While adipocytes were suppressed in irradiated mandible, the irradiated tibia was distinctively marked by adipocytic infiltration ($p < 0.001$) (Fig. 4L). These site-dependent histological features of ORN were consistent when irradiated mandible and tibia were further challenged with minor surgical trauma (Figs. 5A and B); however, micro -CT showed advanced alveolar and periodontal bone loss in irradiated mandible relative to non-irradiated site (Figs. 5C and E). Along this line, minor surgery to irradiated tibia increased the risk of fracture to both irradiated tibia and associated fibula that was otherwise spared from irradiation (Figs. 5D and F).

We used immunostaining to assess skeletal site dependent effects of ionizing radiation. Mechanistically, bone vasculature is vital for maintaining bone marrow stromal cell 'niche' needed to repopulate the pool of osteoprogenitor cells involved in bone healing [5, 19, 20]. Also, VEGF promotes angiogenesis, and bFGF promotes collagen synthesis. Along this line, immunoreactivity of irradiated mandible and tibia with VEGF (Figs. 6A, B, E and F) and bFGF (Figs. 6C, D, G and H) confirmed a reduction in number of immunostained blood vessels relative to non-irradiated left side although this was not significantly different between mandible and tibia (Fig. 6I). Hypoxia and production of MDA have been associated with oxidative stress in radiation damage [21, 22]. Lipid hydroperoxides that accumulate during cellular oxidative stress decompose to form MDA, a thiobarbituric acid reactive substance (TBARS) used to evaluate levels of lipid peroxidation. Therefore, increased levels of MDA epitopes usually correlate with higher lipid peroxidation and oxidative stress. Immunostaining of irradiated mandible relative to control showed higher levels of HIF1α (a marker of hypoxia, Figs. 7A and B) and MDA (an indirect assessment of lipid peroxidation, Figs. 7E and F). Although HIF1α immunoreactivity was also upregulated in irradiated tibia, no differences were seen in degree of MDA immunoreactivity (Figs. 7D, E, G and H).

DISCUSSION

The goal of head and neck cancer radiotherapy is to induce maximum permanent damage to cancer tissues with minimal collateral damage to normal tissues [1, 2, 23]. Despite improvements in irradiation protocols, the jaw bone and salivary glands often receive collateral radiation damage with consequent development of jaw ORN and salivary hypofunction respectively [1–3]. A small animal model of jaw ORN is essential to fully understand cellular events in ORN and develop preventive measures that will minimize morbidity while enhancing cancer survivorship [5]. Since jaw ORN can develop either spontaneously or following dental extraction, [10, 13], previous ORN animal models that were induced by tooth extractions in the irradiated site have not fully illuminated the early cellular events that potentially enhance jaw susceptibility to ORN [1, 10, 16, 17, 24]. In this study, 50 Gy, a clinically-relevant dose delivered using HDR afterloader Unit induced spontaneous jaw ORN independent of surgical trauma [9, 11, 12] and animals that received radiation in the tibia survived long enough for evaluation of radiation outcomes. The added challenge of minor trauma however increased alveolar bone loss and risk of tibial fracture so animals had to be euthanized, further limiting longitudinal follow up. A major reason for using female NIH-RNU rats for the ORN models in this pilot study is because their ability to minimize graft rejection will enable us test graft therapy for ORN in future studies[10, 13]. Female rats also attain skeletal maturity faster than males[25] just like humans[26]. As ossification of rat cranial and appendicular bones occurs about 7–8 days after birth, using 6-week old female rats is an appropriate model to evaluate pathophysiological events of ORN in mature bones [22]

Clinically, ORN is a chronic disorder with a slow onset [1–3]. It begins with an acute phase response to ionizing radiation that consists of erythema due to vascular hyperemia and dermatitis caused by tissue inflammation. ORN gradually progresses into the chronic phase that includes vascular damage leading to thrombosis and tissue fibrosis caused by a combination of cell death and deposition of extracellular collagen [27]. Although the radiation-induced macroscopic tissue changes in the tibia were latent and non-observable by micro-CT, histological analysis revealed trabecular bone breakdown, altered marrow cellular components and adipocytic trans-differentiation typical of bone marrow necrosis [28, 29]. These pathological cellular changes remained subclinical much longer in the tibia but were possibly accelerated in the mandible. The observed tibial response is in accord with enhanced adipocytic differentiation often seen in the long bones of patients with alcohol-induced osteonecrosis [30]. Taken together, these disparate responses between mandible and tibia indicate that onset and course of ORN are apparently skeletal site-dependent.

Radiation promotes release of free radicals like superoxide (O^-) and hydroxyl (OH^-) that play important roles in radiation-induced cell death and delayed healing by inhibiting proliferation of osteoprogenitor cells while stimulating osteoclast proliferation [5, 30, 31]. Radiation damage to vasculature also causes thrombosis and damage to the bone marrow stromal cell (BMSC) 'niche' that provide progenitor cells needed to repair damaged bone. These mechanistic changes of increased hypoxia, hypocellularity and oxidative stress were more demonstrable in irradiated mandible than tibia[7]

Healing of irradiated bone is initiated by BMSCs mobilized from the marrow to the site of injury to provide osteoprogenitor cells [30, 32]; thus delayed or abnormal healing pattern in the mandible relative to tibia may have been precipitated by higher radiation-induced loss of mandibular (orofacial) BMSCs (OFMSCs) as a result of the combined effects of hypoxia, hypovascularity and oxidative stress. This is consistent with earlier reports in humans and rodents that BMSCs are phenotypically and functionally different depending on their skeletal site of origin [12, 33–35]. In same individuals, OFMSCs are highly proliferative with long population doubling times; when irradiated they become slow-cycling cells and remain quiescent much longer than iliac crest BMSCs (ICMSCs) [5, 9]. It is possible that altered cell cycle properties of OFMSCs could translate to stromal cell suppression and dysregulated healing in irradiated jaw making the jaw more susceptible to ORN along a sequence of events that include: 1) hypoxic-hypocellular marrow; 2) hypovascularity; 3) increased adipogenesis and fatty infiltration; 4) delayed healing; 5) trabecular bone breakdown; 6) cortical bone breakdown and finally, 7) accelerated bone breakdown with formation of sequestrum.

Furthermore, minor trauma, high microbial load, damage to teeth and supporting structures are other factors that could complicate jaw ORN and cancer survivorship [36]. A combination of radiation and minor trauma induced further alveolar bone loss in the mandible and increased the risk of tibial fracture. These are consistent with clinical features of ORN often seen in humans. Additionally, mandibular right incisor and first molar of irradiated rats in this study developed necrotic pulp, sclerotic dentin, hypercalcification and ankylosis that may have impacted mastication and erratic weight gain. These sequence of events in our rat model will be logistically impracticable to demonstrate in humans due to ethical reasons, but they are consistent with human clinical conditions where tooth devitalization, delayed eruption patterns and periodontal disease after head and neck radiotherapy make ORN more debilitating [36]. Furthermore, our data affirm that underlying damage to cellular and vascular structures following head and neck cancer radiotherapy apparently work in concert with dental surgery and periodontal disease to advance ORN. Although severity of osteonecrosis can be assessed in histological sections based on loss of viable osteocytes [11, 17], the earliest histological criteria for definitive diagnosis of osteonecrosis are still debatable due to its

multifactorial etiology from radiation, drugs, alcohol, infection and trauma [6, 24, 27, 37]. This pilot study involves a limited number of experimental animals but it is consistent with a previous ORN study that showed that limited sample size can still be used to define skeletal outcomes of radiation [38]. Despite the limited sample size, the outcomes suggest apparent site-disparity in the onset and cellular features of ORN in the jaws relative to long bones with mandible being more susceptible to ORN than tibia. This report also underscore the need for more studies to illuminate skeletal site-dependent effects of radiation-induced hypoxia, hypocellularity, hypovascularity, oxidative stress and trauma in the pathogenesis of ORN.

Acknowledgments

The authors thank Drs. Liu Qing, Faizan Alawi and Muralidhar Mupparapu for their useful comments and Mr. Erik Blankmeyer for technical assistance. This project was supported in part by United Stated Department of Health and Human Services/National Institutes of Health/National Cancer Institute (NIH/NCI) grant 5K08CA120875 and Penn Center for Musculoskeletal Disorders funded by NIH/National Institute of Arthritis, Musculoskeletal and Skin Disorders (NIH/NIAMS) research grant AR050950.

REFERENCES

1. Center for Disease Control. , editor. CDC. National Oral Health Surveillance System-Complete Tooth Loss. 2009 Jun 15. 2010.
2. Fischer DJ, Epstein JB. Management of patients who have undergone head and neck cancer therapy. Dent Clin North Am. 2008 Jan; 52(1):39–60. viii. [PubMed: 18154864]
3. Vissink A, Jansma J, Spijkervet FK, Burlage FR, Coppes RP. Oral sequelae of head and neck radiotherapy. Crit Rev Oral Biol Med. 2003; 14(3):199–212. [PubMed: 12799323]
4. Schou S, Holmstrup P, Worthington HV, Esposito M. Outcome of implant therapy in patients with previous tooth loss due to periodontitis. Clin Oral Implants Res. 2006 Oct; 17(Suppl 2):104–123. [PubMed: 16968387]
5. Cao X, Wu X, Frassica D, Yu B, Pang L, Xian L, et al. Irradiation induces bone injury by damaging bone marrow microenvironment for stem cells. Proceedings of the National Academy of Sciences of the United States of America. 2011 Jan 25; 108(4):1609–1614. [PubMed: 21220327]
6. Marx RE. Osteoradionecrosis: a new concept of its pathophysiology. Journal of oral and maxillofacial surgery : official journal of the American Association of Oral and Maxillofacial Surgeons. 1983 May; 41(5):283–288. [PubMed: 6572704]
7. Yu J, Piao BK, Pei YX, Qi X, Hua BJ. Protective effects of tetrahydropalmatine against gamma-radiation induced damage to human endothelial cells. Life sciences. 2010 Jul 3; 87(1–2):55–63. [PubMed: 20562023]
8. Marx RE. A new concept in the treatment of osteoradionecrosis. J Oral Maxillofac Surg. 1983; 41(6):351–357. [PubMed: 6574217]
9. Damek-Poprawa M, Stefanik D, Levin LM, Akintoye SO. Human bone marrow stromal cells display variable anatomic site-dependent response and recovery from irradiation. Archives of Oral Biology. 2010 May; 55(5):358–364. [PubMed: 20378097]
10. Lerouxel E, Moreau A, Bouler JM, Giumelli B, Daculsi G, Weiss P, et al. Effects of high doses of ionising radiation on bone in rats: a new model for evaluation of bone engineering. The British journal of oral & maxillofacial surgery. 2009 Dec; 47(8):602–607.
11. Kanis JA, Melton LJ 3rd, Christiansen C, Johnston CC, Khaltaev N. The diagnosis of osteoporosis. J Bone Miner Res. 1994 Aug; 9(8):1137–1141. [PubMed: 7976495]
12. Akintoye SO, Lam T, Shi S, Brahim J, Collins MT, Robey PG. Skeletal site-specific characterization of orofacial and iliac crest human bone marrow stromal cells in same individuals. Bone. 2006 Jun; 38(6):758–768. [PubMed: 16403496]
13. Liddelow G, Klineberg I. Patient-related risk factors for implant therapy. A critique of pertinent literature. Aust Dent J. 2011 Dec; 56(4):417–426. quiz 41. [PubMed: 22126353]

14. Feldkamp LA, Davis LC, Kress JW. Practical cone beam algorithm. Journal of the Optical Society of America A: Optics, Image Science, and Vision 1984 June. 1984; 1(6):612–619.
15. Loening AM, Gambhir SS. AMIDE: a free software tool for multimodality medical image analysis. Mol Imaging. 2003 Jul; 2(3):131–137. [PubMed: 14649056]
16. Bone HG, Hosking D, Devogelaer JP, Tucci JR, Emkey RD, Tonino RP, et al. Ten years' experience with alendronate for osteoporosis in postmenopausal women. N Engl J Med. 2004 Mar 18; 350(12):1189–1199. [PubMed: 15028823]
17. Pazianas M, Miller P, Blumentals WA, Bernal M, Kothawala P. A review of the literature on osteonecrosis of the jaw in patients with osteoporosis treated with oral bisphosphonates: prevalence, risk factors, and clinical characteristics. Clin Ther. 2007 Aug; 29(8):1548–1558. [PubMed: 17919538]
18. Tezal M, Wactawski-Wende J, Grossi SG, Ho AW, Dunford R, Genco RJ. The relationship between bone mineral density and periodontitis in postmenopausal women. J Periodontol. 2000 Sep; 71(9):1492–1498. [PubMed: 11022780]
19. Crisan M, Yap S, Casteilla L, Chen CW, Corselli M, Park TS, et al. A perivascular origin for mesenchymal stem cells in multiple human organs. Cell Stem Cell. 2008 Sep 11; 3(3):301–313. [PubMed: 18786417]
20. Shi S, Gronthos S. Perivascular niche of postnatal mesenchymal stem cells in human bone marrow and dental pulp. Journal of bone and mineral research : the official journal of the American Society for Bone and Mineral Research. 2003 Apr; 18(4):696–704. [PubMed: 12674330]
21. Bornstein MM, Cionca N, Mombelli A. Systemic conditions and treatments as risks for implant therapy. Int J Oral Maxillofac Implants. 2009; 24(Suppl):12–27. [PubMed: 19885432]
22. Hughes PC, Tanner JM. The assessment of skeletal maturity in the growing rat. J Anat. 1970 Mar; 106(Pt 2):371–402. [PubMed: 4315144]
23. NIH. The Surgeon General's Report on Bone Health and Osteoporosis: What It Means to You NIH Publication No. 12-7827. Bethesda MD: National Institutes of Health; 2012.
24. Ruggiero SL, Dodson TB, Assael LA, Landesberg R, Marx RE, Mehrotra B. American Association of Oral and Maxillofacial Surgeons position paper on bisphosphonate-related osteonecrosis of the jaws--2009 update. J Oral Maxillofac Surg. 2009 May; 67(5 Suppl):2–12. [PubMed: 19371809]
25. Hughes PC, Tanner JM. A longitudinal study of the growth of the black-hooded rat: methods of measurement and rates of growth for skull, limbs, pelvis, nose-rump and tail lengths. J Anat. 1970 Mar; 106(Pt 2):349–370. [PubMed: 5442228]
26. Tanner, JM.; Whitehouse, RH.; Healy, MJR. A new system for estimating skeletal maturity from the hand and wrist, with standards derived from a study of 2600 healthy British children.Part II. the Scoring System. Paris: International Childrens Center; 1962.
27. Marx RE, Johnson RP. Studies in the radiobiology of osteoradionecrosis and their clinical significance. Oral surgery, oral medicine, and oral pathology. 1987 Oct; 64(4):379–390.
28. Colella G, Campisi G, Fusco V. American Association of Oral and Maxillofacial Surgeons position paper: Bisphosphonate-Related Osteonecrosis of the Jaws-2009 update: the need to refine the BRONJ definition. J Oral Maxillofac Surg. 2009 Dec; 67(12):2698–2699. [PubMed: 19925998]
29. Miyanishi K, Yamamoto T, Irisa T, Yamashita A, Jingushi S, Noguchi Y, et al. Bone marrow fat cell enlargement and a rise in intraosseous pressure in steroid-treated rabbits with osteonecrosis. Bone. 2002 Jan; 30(1):185–190. [PubMed: 11792583]
30. Yeh CH, Chang JK, Ho ML, Chen CH, Wang GJ. Different differentiation of stroma cells from patients with osteonecrosis: a pilot study. Clinical orthopaedics and related research. 2009 Aug; 467(8):2159–2167. [PubMed: 19330390]
31. Garrett IR, Boyce BF, Oreffo RO, Bonewald L, Poser J, Mundy GR. Oxygen-derived free radicals stimulate osteoclastic bone resorption in rodent bone in vitro and in vivo. The Journal of clinical investigation. 1990 Mar; 85(3):632–639. [PubMed: 2312718]
32. FitzGerald TJ, Santucci MA, Harigaya K, Woda B, McKenna M, Sakakeeny MA, et al. Radiosensitivity of permanent human bone marrow stromal cell lines: effect of dose rate. Int J Radiat Oncol Biol Phys. 1988 Nov; 15(5):1153–1159. [PubMed: 3182348]

33. Aghaloo TL, Chaichanasakul T, Bezouglaia O, Kang B, Franco R, Dry SM, et al. Osteogenic potential of mandibular vs. long-bone marrow stromal cells. Journal of Dental Research. 2010 Nov; 89(11):1293–1298. [PubMed: 20811069]
34. Matsubara T, Suardita K, Ishii M, Sugiyama M, Igarashi A, Oda R, et al. Alveolar bone marrow as a cell source for regenerative medicine: differences between alveolar and iliac bone marrow stromal cells. Journal of bone and mineral research : the official journal of the American Society for Bone and Mineral Research. 2005 Mar; 20(3):399–409. [PubMed: 15746984]
35. Yamaza T, Ren G, Akiyama K, Chen C, Shi Y, Shi S. Mouse mandible contains distinctive mesenchymal stem cells. Journal of Dental Research. 2011 Mar; 90(3):317–324. [PubMed: 21076121]
36. Kielbassa AM, Hinkelbein W, Hellwig E, Meyer-Luckel H. Radiation-related damage to dentition. Lancet Oncol. 2006 Apr; 7(4):326–335. [PubMed: 16574548]
37. Sarin J, Derossi SS, Akintoye SO. Updates on bisphosphonates and potential pathobiology of bisphosphonate-induced jaw osteonecrosis. Oral Dis. 2008 May; 14(3):277–285. [PubMed: 18336375]
38. Armin BB, Hokugo A, Nishimura I, Tamplen M, Beumer J 3rd, Steinberg ML, et al. Brachytherapy-mediated bone damage in a rat model investigating maxillary osteoradionecrosis. Arch Otolaryngol Head Neck Surg. 2012 Feb; 138(2):167–171. [PubMed: 22351863]

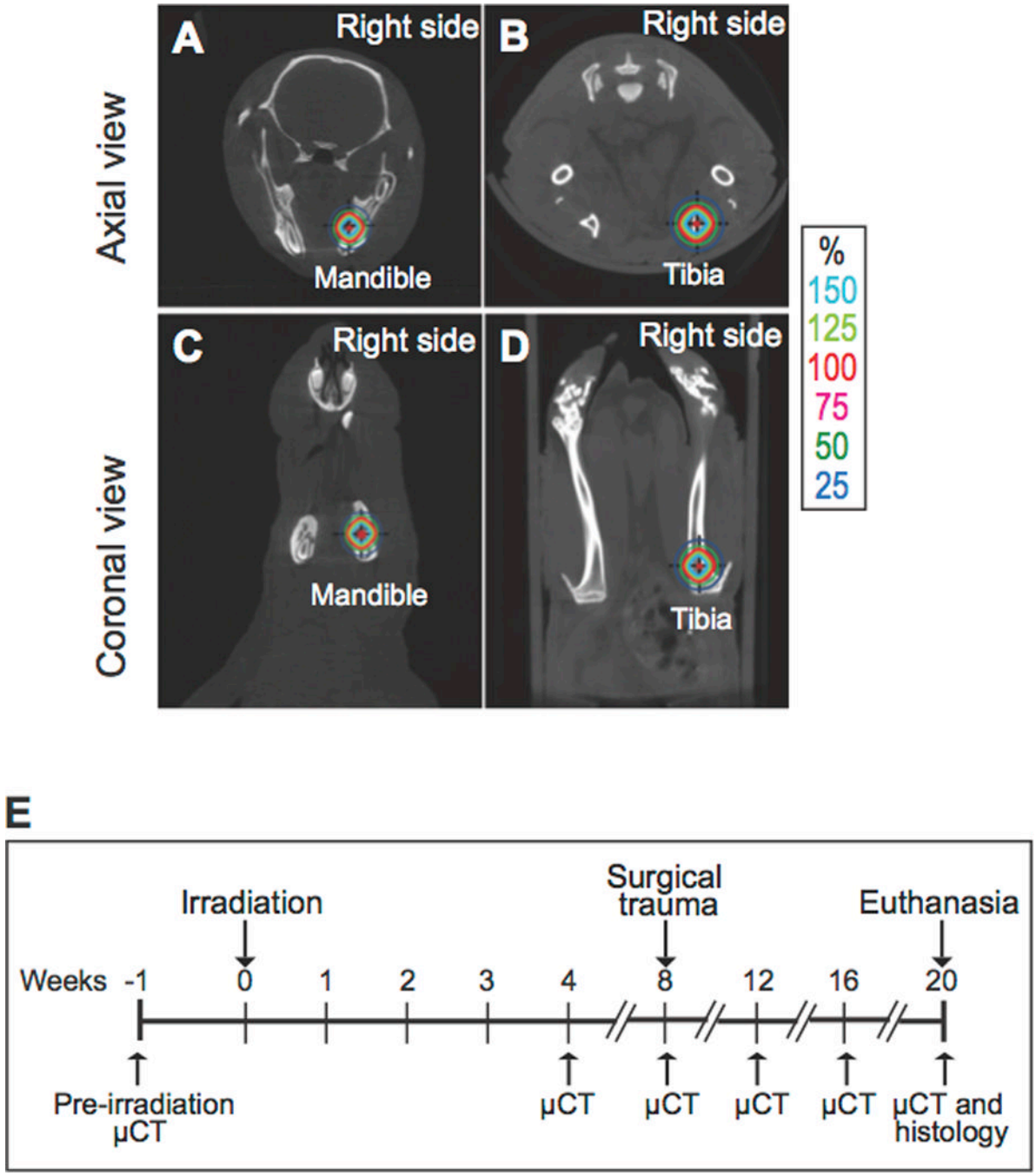

Fig. 1.

Representative micro-CT (µCT) of mandible (A and C) and tibia (B and D) with overlay of 50 Gy isodose on the irradiated (right) side. Note the isodose penetrated the full length of mandible and tibia. Experimental design (E) shows timing of *in vivo* micro-CT and minor surgery.

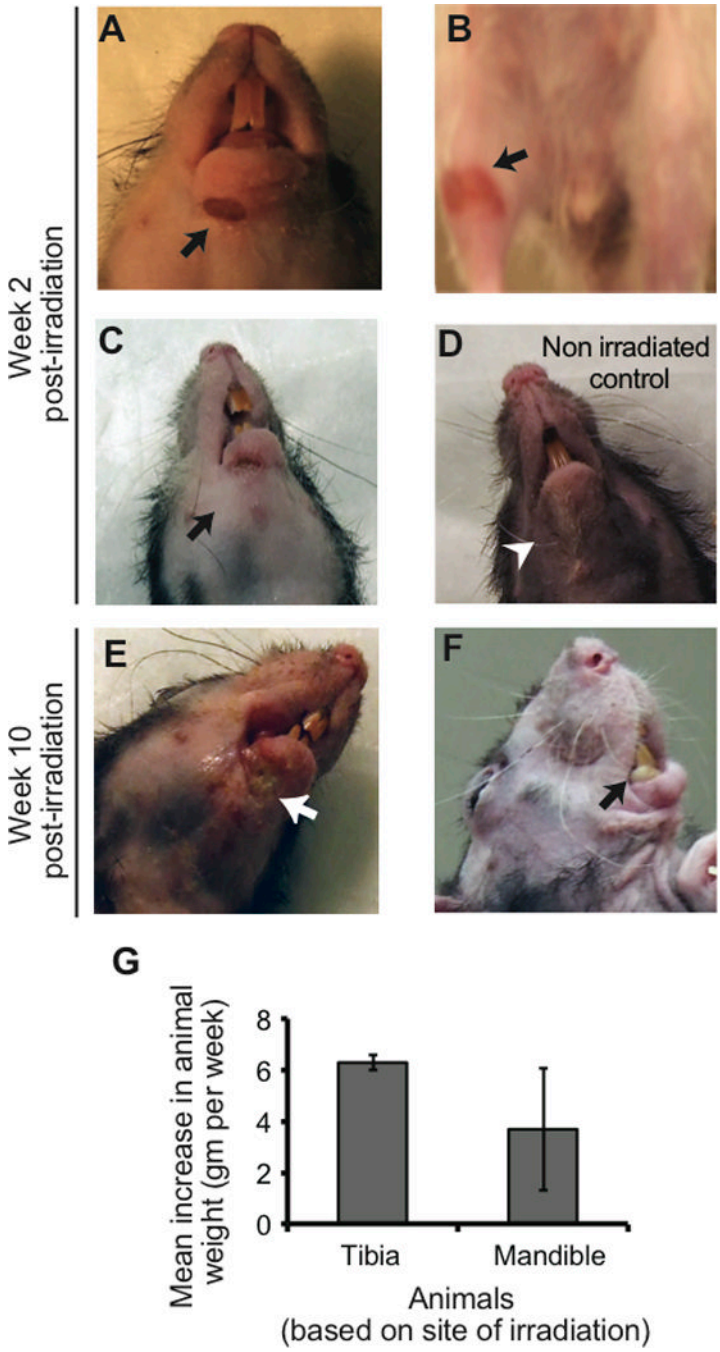

Fig. 2.

Localized radiation outcomes. Mandible (A) and tibia (B) developed localized radiation-induced erythema (black arrows) within the first two weeks post-irradiation. In all animals, associated inflammatory edema was significantly pronounced in the irradiated mandible (C, black arrow) compared to non-irradiated animal (D, white arrow head). Orofacial soft and hard tissues rapidly progressed to necrosis (E, white arrow) and formation of bone sequestrum (F, black arrow) by week 10. Soft tissue overlying irradiated tibia remained intact as shown in B up to week 20. The mean cumulative weight gain of all animals with irradiated mandible was lower and more variable (wide error bars) than those with irradiated tibia [(G) but the differences were not statistically significant].

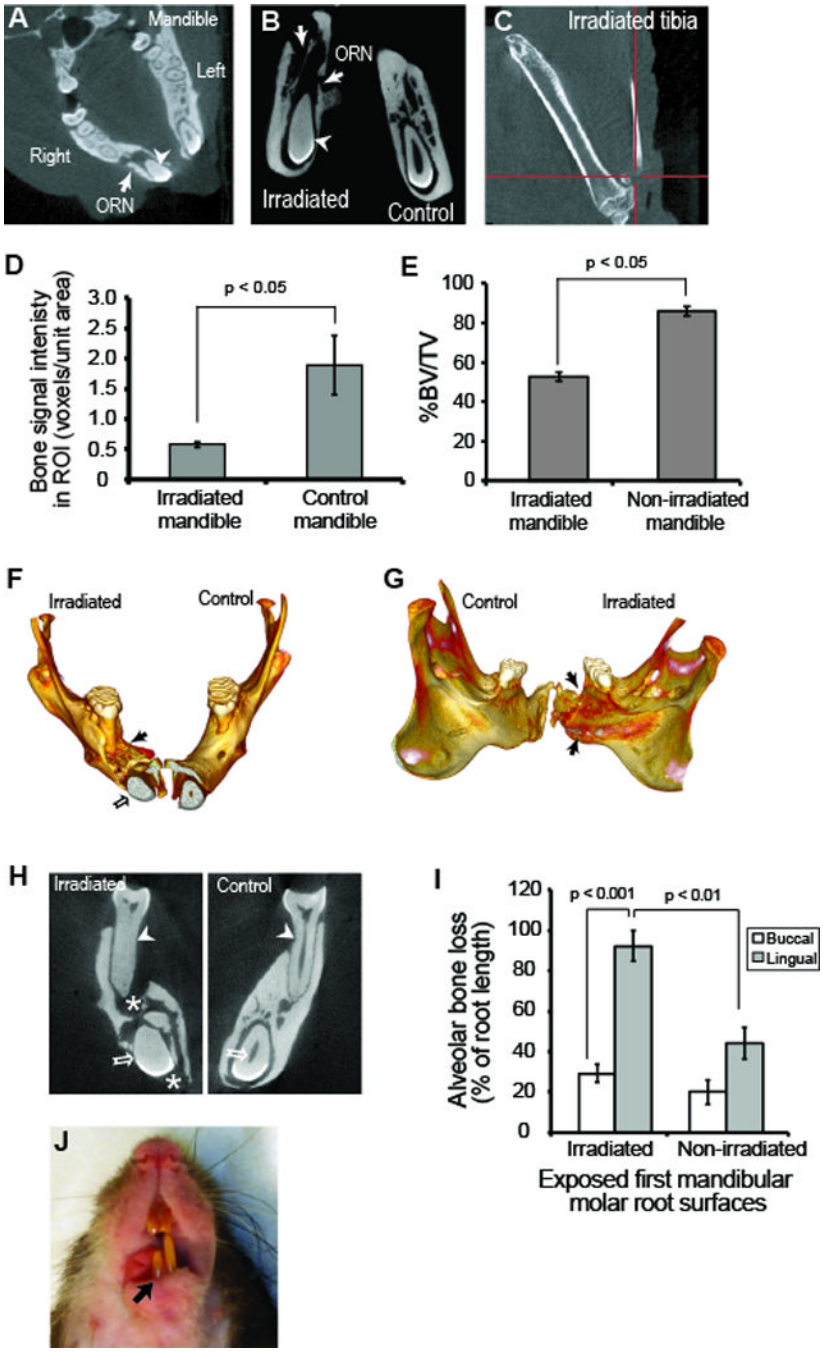

Fig. 3.

Skeletal and dental outcomes of irradiation. Micro-CT showed osteoradionecrosis (ORN, white arrows) and opacification of incisor tooth (white arrowhead) that developed in irradiated right mandible about 10 weeks post-irradiation Non-irradiated (control) left mandible and teeth retained normal anatomical trabecular pattern and patent pulp chamber respectively (A and B). Tibial cortical bone plate remained intact post-irradiation without any radiological signs of ORN up till time of sacrifice at 20 weeks (C). There was marked reduction in bone quantity in irradiated right mandible relative to non-irradiated control left mandible ($P < 0.05$) (D, E). Three dimensional micro-CT volume rendering of mandible demonstrated advanced alveolar bone loss (black arrows, F, G). Representative coronal view

of mandibular ORN at the level of the first molar (H) displayed severe periodontal bone loss (white arrowheads), trabecular bone loss (white star) and pulpal calcification of both molar and long incisor teeth (white arrow and arrowheads). Periodontal bone loss was notably more severe on the lingual than the buccal side in both irradiated ($p < 0.001$) and non-irradiated mandible ($p < 0.01$) (I). There was also delayed eruption of right mandibular incisor relative to the left (J).

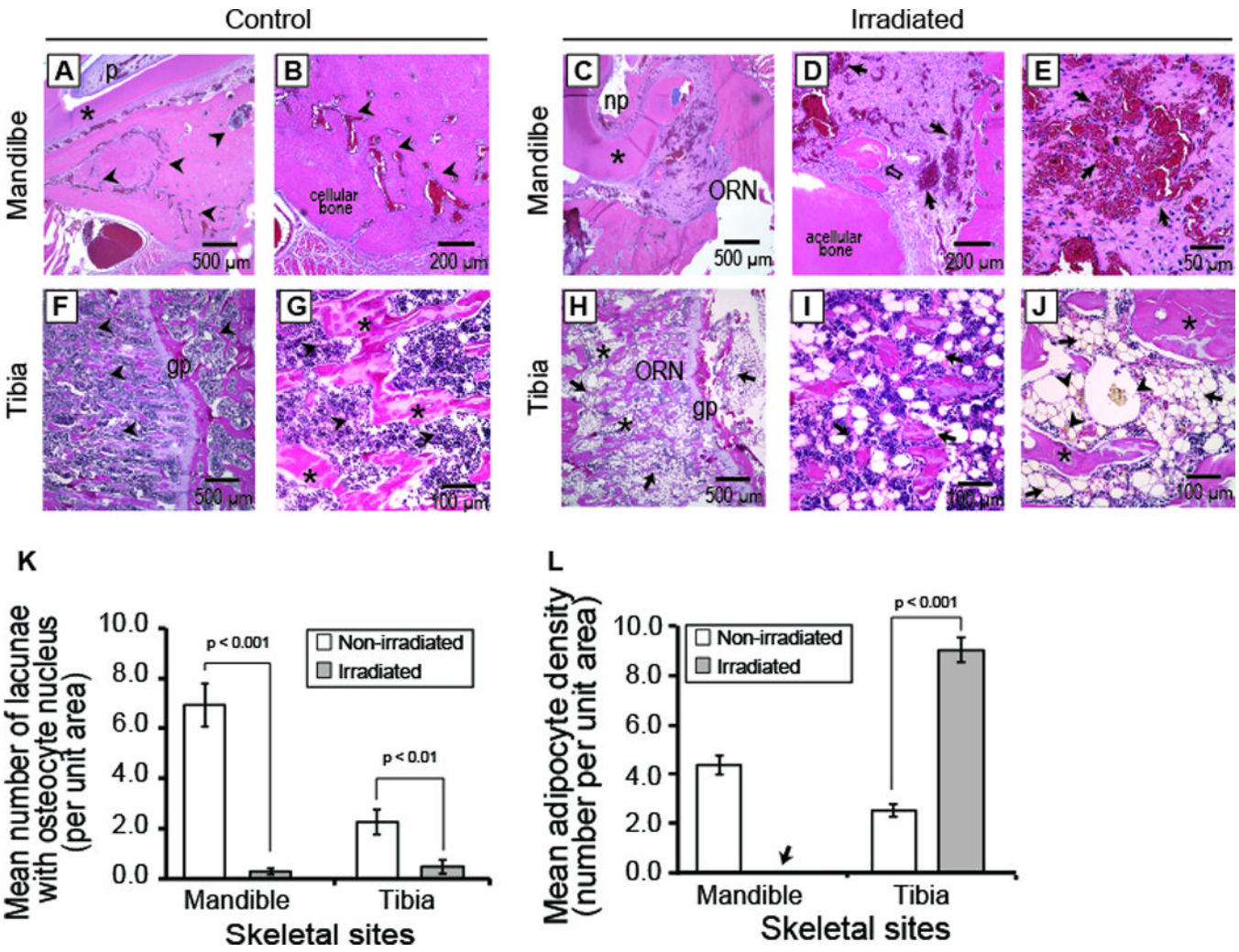

Fig. 4.

Differential histological presentations of mandible and tibia osteoradionecrosis. Non-irradiated mandibular bone (control) (top panel, A, B) displayed a network of normal blood vessels, abundant osteocytes and marrow elements (black arrow heads) in proximity to the mandibular incisor composed of normal dentin (black star) and pulp tissues (p). Similarly, non-irradiated tibia (bottom panel, F, G) displayed abundant marrow elements (arrow heads) and trabecular bone (black star) plus intact growth plate (gp). Irradiated mandible (top panel, C, D, E) succumbed to ORN with characteristic acellular necrotic bone lacking osteocytes, necrotic pulp (np), sequestrum (clear black arrow), and damaged vasculature with erythrocyte extravasation (solid black arrows). The necrotic regions in the mandible were infiltrated by eosinophilic amorphous ground substance with abundant basophilic cells. Radiation damage in tibia (bottom panel, H, I, J) consisted of trabecular micro-fracture with disjointed and fewer trabecular bone (black star), altered architecture of the growth plate (gp), fatty marrow elements (black arrows), coalesced adipocytes and fatty microvesicles (black arrowheads). ORN was associated with empty osteocyte lacunae in both mandible ($p < 0.001$) and tibia ($p < 0.01$) (K); while adipocytes were also suppressed in the mandible (black arrow, L), there was marked adipocytic infiltration in the tibia ($p < 0.001$)(L). [ORN = osteoradionecrosis].

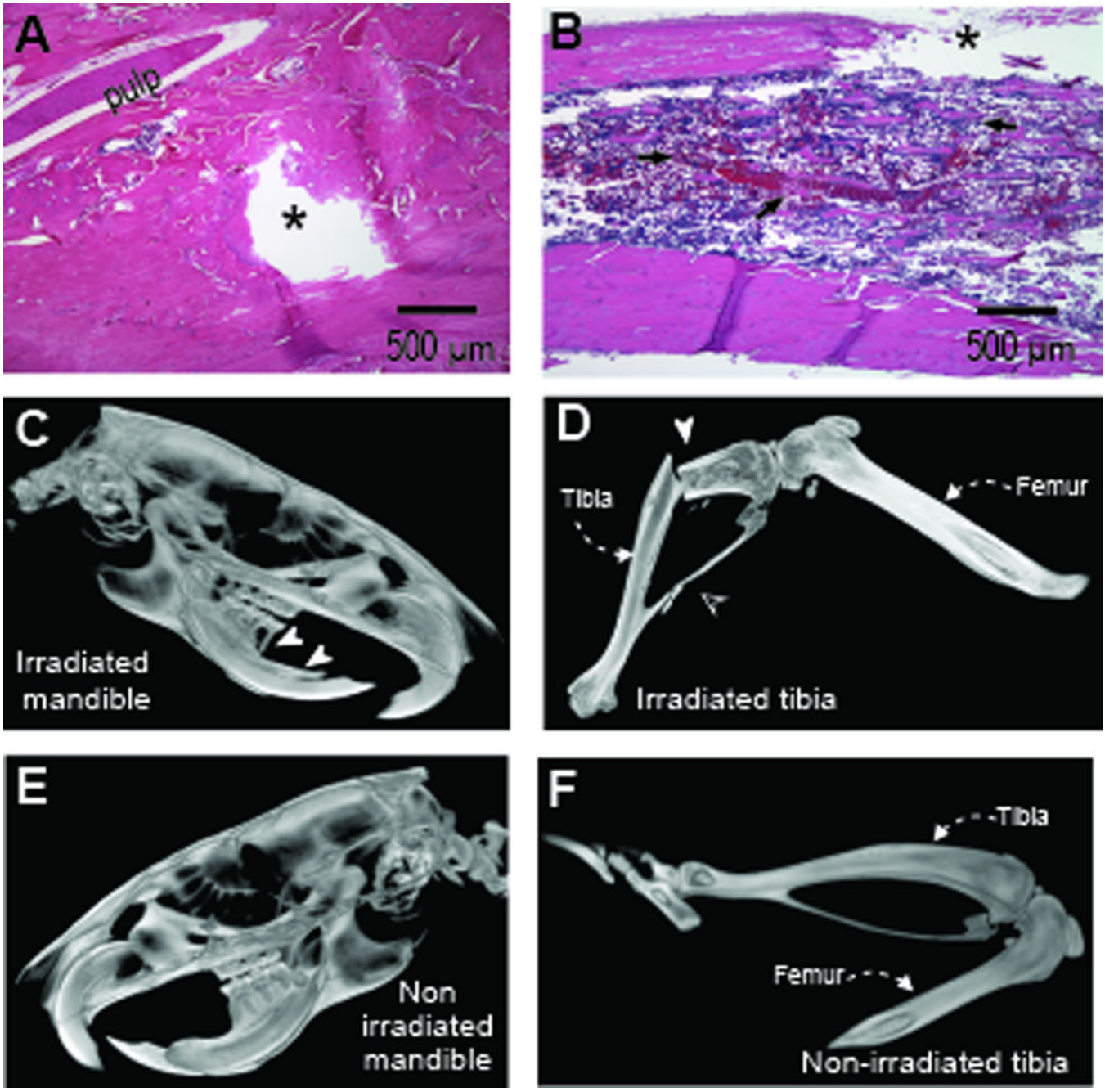

Fig. 5.

Trauma complicates osteoradionecrosis. Hematoxylin and eosin histological sections show trauma-induced cortical window (black star) in irradiated mandible (A) and tibia (B). The irradiated mandible displayed marked acellularity, micro-fractures and pulpal atrophy while tibia displayed disorganized bone trabeculae and adipocytic marrow infiltrates (black arrowheads). Micro-CT volume rendering of irradiated (C and D) and non-irradiated sites (E and F) showed advanced alveolar and periodontal bone loss in irradiated mandible (white arrowheads) relative to non-irradiated site; irradiated tibia with associated fibula succumbed to fracture (white and clear arrowheads respectively).

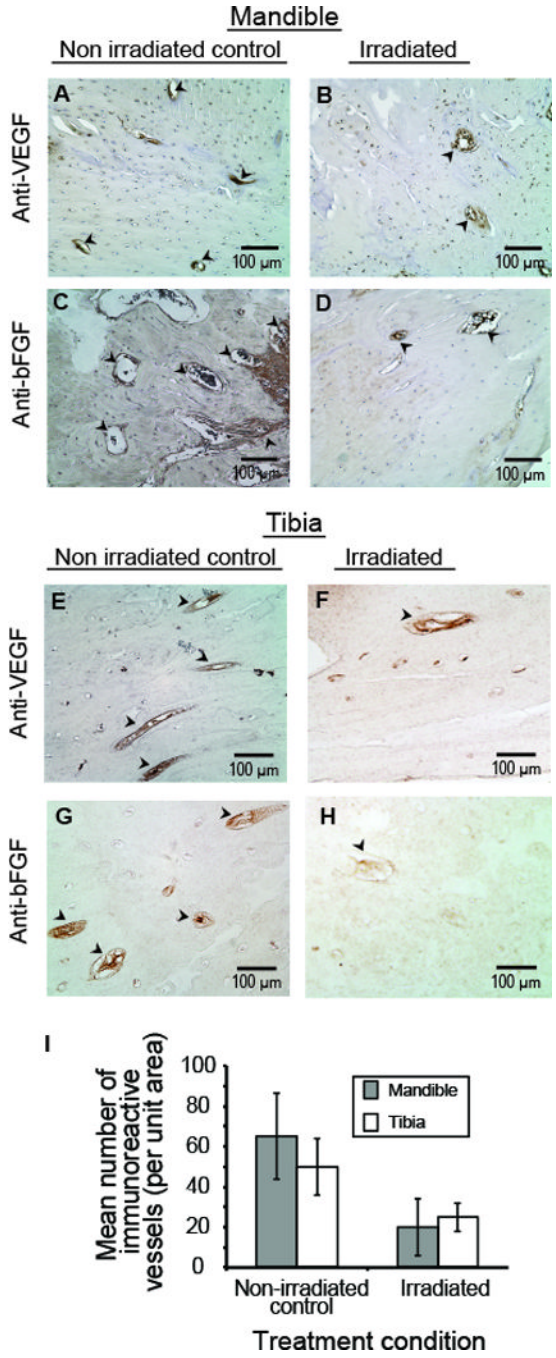

Fig. 6.

Post-irradiation immunoreactive vascular elements. Representative blood vessels immunoreactive to anti-VEGF (A, B, E, F) and anti-bFGF (C, D, G, H) showed a reduction in the number of blood vessels per unit area (black arrowheads) in both irradiated mandible (B, D) and tibia (F, G). Semi-quantitative analysis of immunoreactive vessels (I) showed moderate but non-significant differences between mandible and tibia.

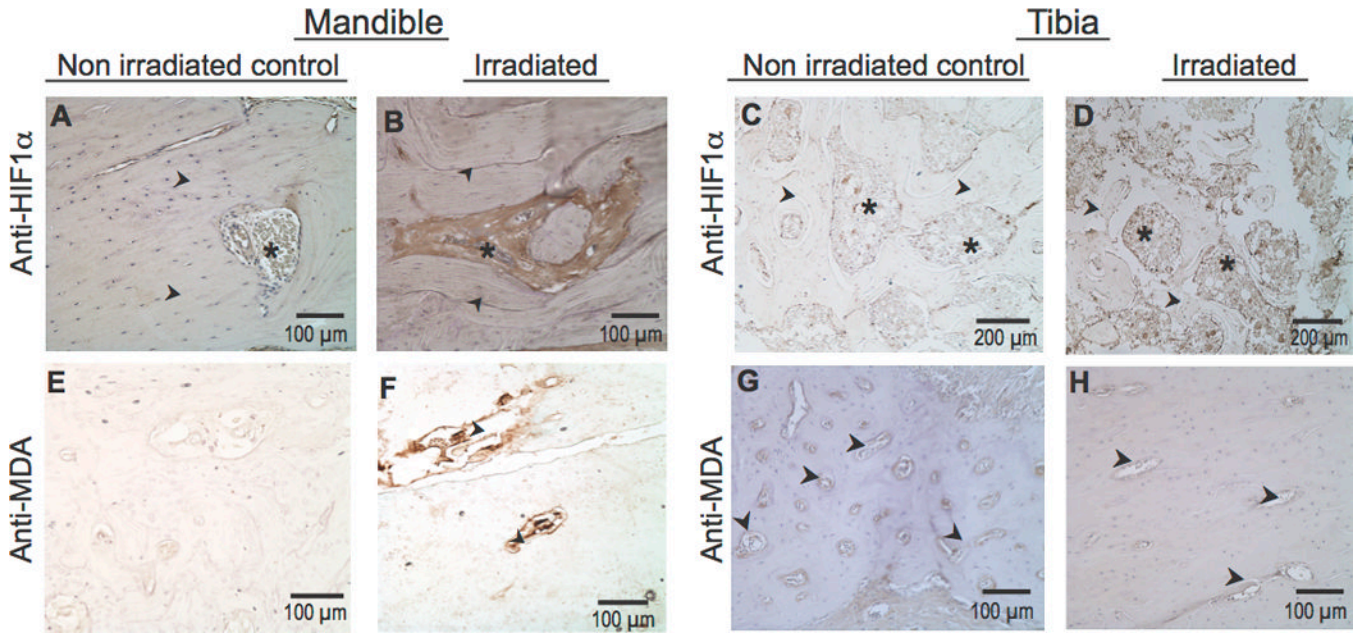

Fig. 7.

Radiation-related hypoxia and oxidative stress. Relative to non-irradiated bone (A, C), hypoxia was upregulated in irradiated mandible (B) and tibia (D) based on stronger Immunoreactivity to HIF1α in the bone trabeculae (black arrowheads) and marrow elements (black stars). Unlike the tibia, irradiated mandibular vasculature was highly immunoreactive (black arrowheads) to anti-MDA relative to non-irradiated mandible (E, F, G, H).